Wafer bow in diamond heteroepitaxy: causes, their analytical description, and viable solutions

Matthias Schreck, Theodor Peter

Angaben zur Veröffentlichung / Publication details:

Schreck, Matthias, and Theodor Peter. 2025. "Wafer bow in diamond heteroepitaxy: causes, their analytical description, and viable solutions." Journal of Applied Physics 137 (1): 015108. https://doi.org/10.1063/5.0245362.

Journal of Applied Physics

RESEARCH ARTICLE | JANUARY 07 2025

Wafer bow in diamond heteroepitaxy: Causes, their analytical description, and viable solutions

Matthias Schreck ; Theodor Peter

J. Appl. Phys. 137, 015108 (2025)
https://doi.org/10.1063/5.0245362

Journal of Applied Physics ARTICLE pubs.aip.org/aip/jap

Wafer bow in diamond heteroepitaxy: Causes, their analytical description, and viable solutions

Cite as: J. Appl. Phys. **137**, 015108 (2025); doi: 10.1063/5.0245362
Submitted: 25 October 2024 · Accepted: 16 December 2024 ·
Published Online: 7 January 2025

Matthias Schreck[a] and Theodor Peter

AFFILIATIONS

Institut für Physik, Universität Augsburg, D-86135 Augsburg, Germany

[a]**Author to whom correspondence should be addressed:** matthias.schreck@physik.uni-augsburg.de. **Tel.:** +49-821-598-3401, **Fax:** +49-821-598-3425

ABSTRACT

Wafer bow is of considerable technological relevance for virtually all semiconductor materials grown by heteroepitaxy. In the case of diamond, the reported curvature values are exceptionally large for synthesis by plasma chemical vapor deposition on oxide substrates. In contrast to the usual explanation by differences in coefficients of thermal expansion (CTEs), the present analysis reveals that the CTE α of the substrate combined with its thermal conductivity λ controls the radius of the surface on which the diamond layer will grow. The ratio λ/α represents a figure of merit for the choice of favorable substrates facilitating maximum flatness. Calculated radii under typical process conditions fit with literature reports. Bow values exceeding these predictions significantly are attributed to the formation of intrinsic stress in diamond according to the effective climb of dislocations mechanism. Stress profiles inside of thick diamond layers after the removal of the substrate are calculated based on this mechanism taking into consideration the experimentally observed decrease in the dislocation density. They predict compressive stress in the center and tensile stress at the nucleation as well as at the growth surface in accordance with literature reports and Raman measurements. High intrinsic stress in the growing film can heavily deform the growth substrate provided that the deposition temperature is above its brittle/ductile transition. In all cases, deformation caused by extrinsic stress occurring during cool-down is =apparently of minor relevance. Two alternative strategies for the achievement of flat wafers are presented.

I. INTRODUCTION

Due to its unique material parameters, diamond is considered the ultimate wide bandgap semiconductor material.[1] To harness its beneficial properties, high quality single crystals in technologically relevant wafer dimensions are required. In spite of appreciable work during the last decades, the growth of bulk crystals by the high-pressure high-temperature (HPHT) method is still limited to less than $15 \times 15\,\mathrm{mm}^2$.[2] Efforts in chemical vapor deposition (CVD) in combination with heteroepitaxy on appropriate foreign single crystals were more successful. First, iridium was identified as the unique material, which facilitates the generation of diamond nuclei with ultrahigh density and excellent alignment on its surface by the bias enhanced nucleation (BEN) procedure. Then, different scalable substrates such as MgO, $SrTiO_3$, Al_2O_3, $SrTiO_3$/Si, and YSZ/Si were found on which Ir films could be grown in single crystal quality. While the Ir/metal oxide combinations profit from a simpler preparation process, the silicon-based multilayer structure diamond/Ir/YSZ/Si has enabled the largest diamond wafers until now.[3]

Besides structural quality, excellent wafer flatness is imperative when lithographic patterning steps are applied to generate micron-size device structures. Polishing is, therefore, a standard procedure after deposition. However, besides the expenditure of time and loss of the valuable material, this approach completely fails when the bow is higher than the thickness of the grown diamond layer. For freestanding diamond grown on Ir/YSZ/Si, bending radii R are typically on the order of 5 m,[4–6] equivalent to ≈0.25 mm bulge in the center of a 100 mm wafer. In contrast, researchers measured R = 0.2 m (Ref. 7) and ∼0.12 m (Ref. 8) for diamond grown on Ir/MgO. Finally, for diamond deposited on Ir/Al_2O_3 substrates, R values of 0.906,[7] 0.996 (along Al_2O_3[1100]),[9] 2.602 m (along Al_2O_3[0001])[9] were reported. The latter value was derived from a 6 mm-long trace on a selected region of a 2 in. wafer.

As an explanation for the strong curvature, the difference in coefficient of thermal expansion (CTEs) between diamond and the oxide

substrates is most commonly put forward.[7,9,10] According to this interpretation, the diamond layer is virtually flat till the end of the growth process. It undergoes convex bending (surface profile is higher in the center) during cooldown induced by the stress imposed by the stronger shrinkage of the substrate compared to the diamond on top. Some residual strain measured in the freestanding diamond substrates was attributed to lattice misfit and grain coarsening effects during growth.[10]

For the heteroepitaxial deposition of other wide bandgap semiconductor materials like GaN, Al_2O_3 is also a common substrate. Freestanding wafers are fabricated by liftoff after growth to a thickness of several hundred mircrometers.[11,12] Before liftoff, the surface of the GaN films on Al_2O_3 usually shows a convex shape, which changes to concave after separation.[12,13] The convex shape of the GaN/Al_2O_3 heterostructure is attributed to and roughly conform with the difference in CTEs. In detail, this means strong bending with R down to 0.6,[12] 0.8,[11] and 0.4 m[13] after deposition and significantly lower bow with opposite sign after liftoff, e.g., $R = 4$ m,[11] and up to 6 m.[12,13] The residual bow is not yet fully explained, but dislocation gradients and nonhomogeneous distributions of point defects are suggested.[13] Most importantly, the radii for freestanding GaN grown on sapphire are in a technologically acceptable range, in contrast to diamond synthesized on this substrate.

While the substrate temperatures during the deposition of diamond and GaN are quite similar (≈1000 °C), the crucial difference consists in the technique used to induce the chemical processes responsible for the deposition. In the case of GaN, heat is delivered from the heater through the wafer to the wafer surface where the precursor molecules are cracked. As a consequence, a small temperature gradient in the range of a few degree Celsius (2 °C as derived by *in situ* measurements) is established between the wafer backside and surface during growth resulting in a concave bending with R = 25 m.[14] In contrast, the typical microwave plasma CVD (MWPCVD) for diamond synthesis has a gas temperature in the center of the plasma ball in the range of 2200–3600 K.[15] This temperature scales with the pressure between 50 and 300 mbar. An appreciable fraction of the dissipated heat will flow toward the growth surface and has to pass through the substrate wafer to the cooling stage. A temperature gradient with opposite sign and convex bending will result.

In the following, the described situation will be analyzed for realistic process conditions and different substrate materials. The results will be compared with the experimental results reported in the literature and data acquired in the authors' lab. Furthermore, modifications generated by the development of intrinsic stress and the role of the plasticity of diamond and the substrate are considered. Simulations are compared with literature reports and μ-Raman measurements. Finally, two concepts are suggested, which can solve the problem and provide flat wafers even on oxide substrates.

II. CALCULATIONS OF THE ELASTIC BENDING FOR DIFFERENT SUBSTRATE MATERIALS DURING MWPCVD

The typical peak temperature of ≥3000 K in the center of the plasma ball during MWPCVD has to decrease to ≈1300 K at the substrate surface within few millimeters.[15] According to this huge gradient, a permanent heat flow is directed toward the surface. In addition to minor radiation loss, the predominant fraction of this heat has to pass from the growth surface through the substrate to the backside of the wafer. The heat flow establishes a temperature gradient inside the wafer, which will cause a convex bending (convex refers to the shape of the top surface). The diamond layer grows on top of this curved surface and will keep this shape after cooldown. The schema in Fig. 1 describes the situation and the resulting shape of the diamond layer.

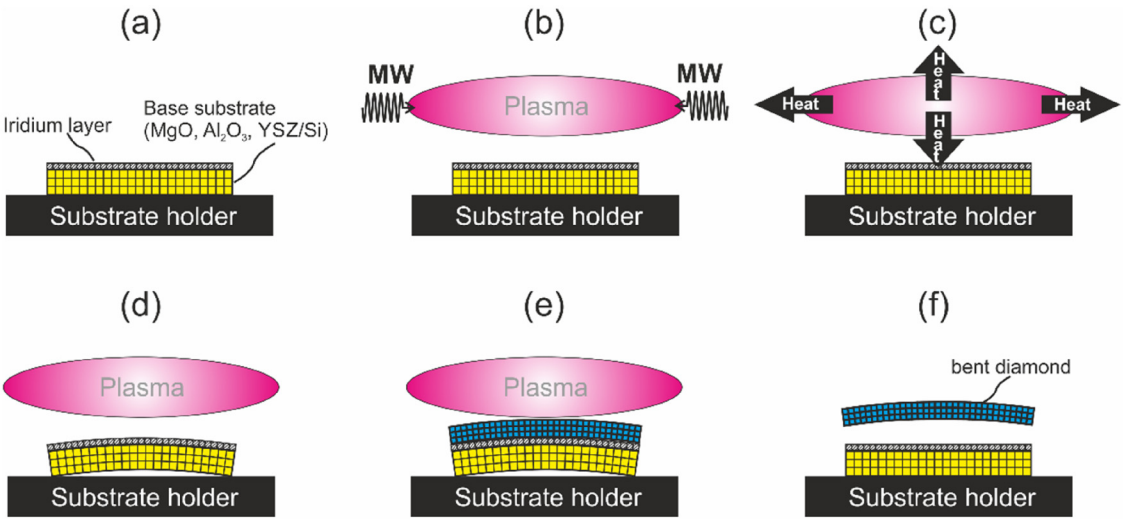

FIG. 1. Schematic description of the growth of bent diamond layers in high-power plasmas. (a) The flat substrate, (b) ignition of the plasma by injection of microwaves, (c) heat transport from the plasma toward reactor walls and substrate surface, (d) the convex bending of the substrate surface caused by heat flow to the substrate holder, (e) the growth of epitaxial diamond layer on the bent iridium surface, (f) the back bending of the substrate after microwave shut down and cooling to room temperature. All deformation processes are considered purely elastic, i.e., substrate bending is reversible, and diamond growth occurs stress-free.

The deformation of the substrate under plasma conditions can be calculated straightforwardly provided that two quantities are known: the surface temperature $T_{surface}$ and the vertical heat flow J through the substrate. The surface temperature is an important process control parameter, and its choice is strongly restricted by the mandatory requirements for high crystal quality and high growth rate. Therefore, $T_{surface} \approx 1000\ ^\circ C$ as a typical value represents one fixed point.

The heat flow J depends primarily on the plasma temperature, which, in turn, is predominantly controlled by the process gas pressure. For a homogeneous plasma in contact with a wafer size substrate that covers roughly the whole sample holder, a meaningful value can be derived by measurement of the heat removed from the sample holder by the cooling water. A rough number determined for growth on 100 mm wafers is 30% of the microwave power injected into the reactor.

When the temperature dependent thermal conductivity λ(T) is known, the temperature profile $T(z)$ inside the wafer can then be calculated for a given $T_{surface}$ and J by integrating Eq. (1) from the surface $z_{surface} = 0$ to $z_{backside} = d$ with d, the wafer thickness,

$$dT = -\frac{1}{\lambda(T)} J dz, \tag{1}$$

$$\frac{dT}{dz} = -\frac{J}{\lambda(T)}. \tag{2}$$

The appreciable uncertainty of the literature values for the thermal conductivity at 1000 °C justifies working with a constant value $\lambda(T) = \lambda(T_{surface})$. As a consequence, the solution of Eq. (1) yields

$$T(z) = T_{surface} - \frac{J}{\lambda(T_{surface})} z, \tag{3}$$

and the temperature difference ΔT between the surface and backside is

$$\Delta T = T_{surface} - T_{backside} = \frac{J}{\lambda(T_{surface})} d. \tag{4}$$

The infinitesimal horizontal length change of the wafer in the plane z, resulting from the linear temperature profile $T(z)$ is given by

$$dL(z) = \alpha(z) \frac{dT}{dz} dz\ L(z), \tag{5}$$

$$\frac{dL(z)}{L(z)} = -\frac{\alpha(z)}{\lambda} J dz. \tag{6}$$

With a constant α and the usual linear approximation for the resulting exponential function, we obtain

$$L(z) = L_0 \left(1 - \frac{\alpha}{\lambda} J z\right). \tag{7}$$

Since neighboring layers z_n and z_{n+1} are attached to each other, the difference in expansion causes forces at the interface. In the case of free bending, the sample counteracts the resulting stress by bending.

The circumference U of a circle with radius $R = R_0 + \Delta R$ can be written as

$$U(R) = 2\pi R = 2\pi(R_0 + \Delta R) = 2\pi R_0 \left(1 + \frac{\Delta R}{R_0}\right). \tag{8}$$

Combining (7) and (8) yields

$$\frac{\Delta R}{R_0} = -\frac{\alpha}{\lambda} J z, \tag{9}$$

and with $\Delta R = -z$,

$$\frac{1}{R_0} = \frac{\alpha}{\lambda} J. \tag{10}$$

According to Eq. (10), the radius increases with the heat conductivity λ and decreases with the heat flux J and the expansion coefficient α. The ratio λ/α is a figure of merit for the selection of substrates guaranteeing a minimum curvature. As shown in Table I, diamond itself would be optimum ($\lambda/\alpha = 78 \times 10^6$ W/m). From the studied heterosubstrates, silicon (5.44×10^6 W/m) outperforms the two oxide substrates Al_2O_3 (0.61×10^6 W/m) and MgO (0.51×10^6 W/m) by roughly one order of magnitude. Since Eq. (10) is independent of the wafer thickness d, the choice of extraordinarily thick crystals would not improve the situation.

Figure 2 shows the calculations of the curvature $1/R$ as a function of heat flux density through the wafer.

As already mentioned in Sec. I, the samples grown in our lab typically show maximum radii around 5 m. Maximum radii means that an appreciable fraction of all crystals are bent stronger in a complex way (twisted), which is attributed to plastic processes in Si. This aspect will be discussed in more detail later. The heat flux density deduced by the measurement of cooling water temperature change and flow rate is $\approx 10^6$ W/m^2. Thus, experiment and calculation coincide within experimental errors.

For all the samples grown on the oxide substrates in foreign laboratories, information on the heat flux density is not available. The radii of 0.906 and 0.996 m for diamond grown on Ir/Al_2O_3(11$\bar{2}$0) suggest a slightly lower heat flux during growth. In contrary, on MgO, the radii of 0.25 and 0.12 m for diamond synthesized on Ir/MgO are much lower than in the calculation (0.51 m). Attributing this to heat flux densities of 2.5×10^6 or 4.25×10^6 W/m^2 is implausible. Actually, the authors who reported 0.12 m for the thick delaminated diamond samples had also performed *in situ* curvature measurements for the MgO wafer under plasma conditions before and at the early stage of diamond growth.[8] There they measured at 1300 K a curvature of 1.1 1/m equivalent to a radius of 0.91 m. This is in a reasonable range and can be attributed to a heat flux density of $\approx 0.56 \times 10^6$ W/m^2.

In order to visualize also the influence on the wafer flatness, the height of the bulge in the center of a 100 mm-diameter wafer has been calculated (see Fig. 3).

The data in Fig. 3 show that the bulge in the center of a 100 mm-diameter diamond wafer grown under conditions, which

TABLE I. Summary of the relevant material parameters for the most common substrates at room temperature (RT) and at 1000 °C.

Material	λ (RT) (W/mK)	λ (1000 °C) (W/mK)	α (RT) ($\times 10^{-6}$ 1/K)	α (1000 °C) ($\times 10^{-6}$ 1/K)	λ/α (1000 °C) ($\times 10^{6}$W/m)
Si	150[a]	24.7[a]	2.56[b]	4.54[b]	5.44
Al_2O_3(av.)	40[c]	6[c]	5.3[b]	9.78[b]	0.61
Al_2O_3(*a*-axis)		||	5.06[b]	9.5[b]	0.63
Al_2O_3(*c*-axis)		||	5.8[b]	10.4[b]	0.58
MgO	50[d]	8[d]	10.5[e]	15.6[e]	0.51
Diamond	2500[f]	400[f]	1.0[e]	5.15[e]	78

[a] λ_{Si}[16]
[b] α_{Si}, $\alpha_{Al_2O_3}$[17]
[c] $\lambda_{Al_2O_3}$[18]
[d] λ_{MgO}[19]
[e] α_{MgO}, α_{Dia}[20]
[f] λ_{Dia}.[21]

produce a heat flux density of $\approx 1 \times 10^6$ W/m^2 on a Si base substrate, would be in an acceptable range (0.23 mm) although it would also require intensive polishing. On the oxide substrates, the bulge of more than 2 mm would be prohibitively high.

III. GROWTH STRESS AND ITS INFLUENCE ON WAFER BENDING

Since deposition occurs at elevated temperatures, extrinsic stress caused by mismatch in CTEs will always occur during cool-down to room temperatures. Its influence on the final curvature will be discussed later in Sec. V. Before, the role of intrinsic stress created during crystal growth will be analyzed. It is also called growth stress.

Various review articles[22–24] have addressed the different mechanisms responsible for the appearance of growth stress, like the attractive interaction at grain boundaries in polycrystalline films described by the "grain boundary relaxation model."[25] This interaction typically results in tensile stress. In contrast, the "atomic peening effect" under the bombardment by energetic particles densifies the deposit and causes compressive stress.

During the growth of heteroepitaxial or even homoepitaxial diamond films, huge stress has also been found, which could not be explained by the previous models. For instance, Mermoux *et al.* measured the tensile stress of several GPa by μ-Raman and

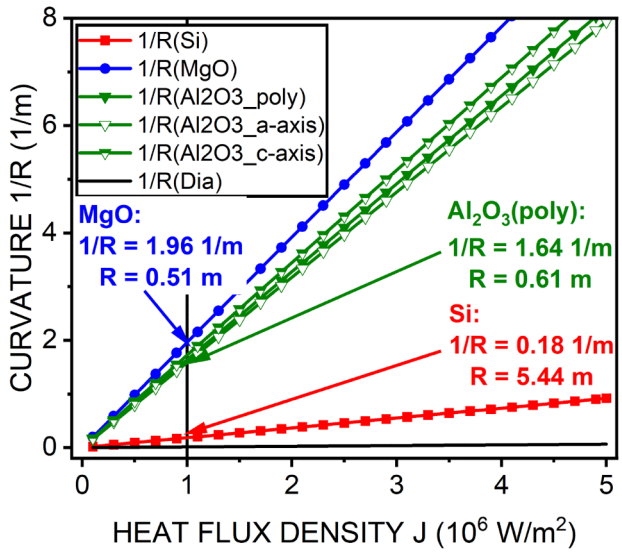

FIG. 2. Curvature 1/R of different substrate materials vs heat flux density through the wafer. For the hexagonal sapphire, the average thermal conductivity was used in all cases. For *c*-plane wafers, α along the *a*-axis is relevant to calculate the curvature. For wafers with the in-plane *c*-axis, two different radii will appear, i.e., a lower radius along the *c*-axis ($\alpha_c = 10.4 \times 10^{-6}$ K^{-1}) and a higher radius in the perpendicular direction given by ($\alpha_a = 9.5 \times 10^{-6}$ K^{-1}).

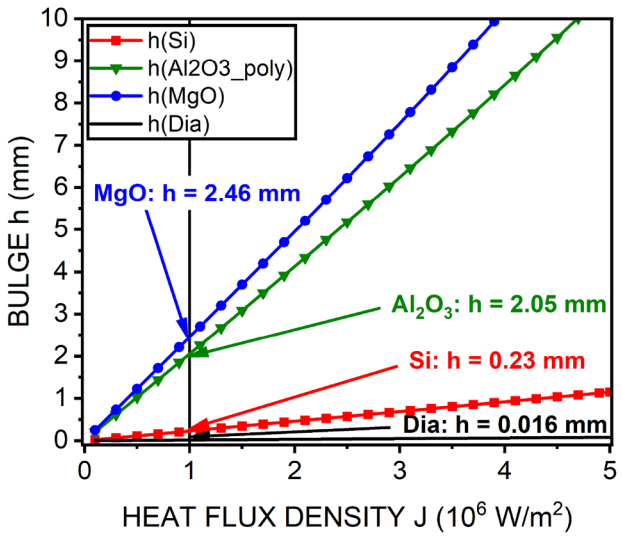

FIG. 3. Height of the bulge in the center of 100 mm-diameter wafers after growth and detachment for different base substrate materials vs the heat flux density through the substrate.

observed the formation of cracks in homoepitaxial diamond films on (111) surfaces.[26] In a systematic study[27] using homo- and heteroepitaxial films, it was later revealed that the formation of growth stress can be varied monotonically in amplitude and in sign starting from below –5 GPa compressive stress at low deposition temperature over vanishing growth stress up to several GPa tensile stress at high deposition temperature. The curve derived on (001) surfaces shifts to higher temperatures on (111) surfaces. The zero-crossing found on both surfaces suggests that vanishing growth stress can be achieved by the selection of the appropriate deposition temperature. However, this is only true for highly symmetric growth planes. In contrast, for (111) off-axis growth, highly asymmetric stress tensors containing simultaneously positive and negative eigenvalues for the two principal in-plane tensor axes have been measured.[28] This usually impedes growth conditions that yield zero stress simultaneously for all tensor components. As a final observation of high relevance, a systematic scaling of the stress amplitude with the dislocation density n_{dis} has been found.[29] For all these effects, the mechanism of "effective climb of dislocations" provides a convincing explanation as also confirmed by transmission electron microscopy (TEM) studies.[30]

According to this mechanism, the dislocations tilt in a direction so that the surface area A (given by the number of lattice cells at the surface and the area a_0^2 of the standard unit cell) increases or decreases monotonically with z being the position along the growth axis,

$$\frac{dA}{dz} = \frac{fA_0 n_{\mathrm{dis}}(0)\frac{1}{2}a_0^2}{a_0} = \frac{1}{2} fA_0 n_{\mathrm{dis}}(0) a_0. \tag{11}$$

Here, a_0 is the lattice constant of the diamond volume cell (0.3567 nm) and f is a numerical constant with $|f| < 1$. Every dislocation increases (or decreases in the case of the opposite tilt direction) the surface area by $f\,\frac{1}{2}a_0^2$ when the thickness increases by a_0. A_0 is the initial surface area and $A_0 n_{dis}(0)$ is the total number of threading dislocations in the sample emerging at the growth surface. A_0 is constant, while A increases (or decreases) slowly with z.

Integration yields

$$A(z) = A_0 + \frac{1}{2} fA_0 n_{\mathrm{dis}}(0) a_0 z = A_0\left(1 + \frac{1}{2} f n_{\mathrm{dis}}(0) a_0 z\right), \tag{12}$$

$$\frac{\frac{dA}{dz}}{A_0} = \frac{1}{2} f n_{\mathrm{dis}}(0) a_0 = \text{const.} \tag{13}$$

The surface S of a spherical shell with inner radius R_0 and outer radius $R = R_0 + z$ is

$$S = 4\pi R^2 = 4\pi(R_0 + z)^2 = 4\pi(R_0^2 + 2R_0 z + z^2) = S_0 + 4\pi(2R_0 z + z^2), \tag{14}$$

$$\frac{\frac{dS}{dz}}{S_0} = \frac{4\pi(2R_0 + 2z)}{4\pi R_0^2} = \frac{2}{R_0}\left(1 + \frac{z}{R_0}\right). \tag{15}$$

For $z \ll R_0$, the radius is

$$R = \frac{4}{f n_{\mathrm{dis}}(0) a_0}. \tag{16}$$

Assuming $f = 1$ and a constant number of dislocations $A_0 n_{\mathrm{dis}}(0)$ inside the growing layer with an initial density of $n_{\mathrm{dis}}(z = 0) = 10^8\ \mathrm{cm}^{-2}$, two extreme cases are to be considered:

(1) Diamond grows on top of an infinitely soft substrate, which is equivalent to "free deflection." The resulting radius is then

$$R = \frac{4}{n_{\mathrm{dis}}(0) a_0} = \frac{4}{10^8\ \mathrm{cm}^{-2} \times 3.567 \times 10^{-8}\ \mathrm{cm}} = 1.21\ \mathrm{cm}.$$

This R has a constant value if no annihilation, merging or new nucleation of dislocations occurs. For small z, the bending avoids any stress inside the layer. For large z, the second term in Eq. (15) gets some relevance and minor stress can develop.

(2) Diamond grows on top of an infinitely stiff substrate equivalent to "inhibited deflection and expansion." The symmetric in-plane strain ε_{xx} that is built up at a thickness z is then given by

$$\frac{\Delta A}{A_0} = \frac{1}{2} n_{\mathrm{dis}}(0) a_0 z = -\frac{\Delta x}{x} - \frac{\Delta y}{y} = -\varepsilon_{xx} - \varepsilon_{yy} = -2\varepsilon_{xx}. \tag{17}$$

Here, we use the definition that an increase in the number of lattice cells causes a compression, i.e., negative strain and stress.

To generate a biaxial stress of $\sigma_{xx} = -1$ GPa, a biaxial strain

$$\varepsilon_{xx} = (s_{11} + s_{12})\sigma_{xx}, = -(0.9524 - 0.09913) \times 10^{-12}\,\frac{1}{\mathrm{Pa}} \times 10^9\ \mathrm{Pa} = -0.853 \times 10^{-3} \tag{18}$$

is needed. s_{11} and s_{12} are the components of diamond's compliance tensor.

In order to find this stress level in the last monolayer deposited, a thickness of

$$\frac{4 \times 0.853 \times 10^{-3}}{10^8\ \mathrm{cm}^{-2} \times 3.567 \times 10^{-8}\ \mathrm{cm}} = 0.9568 \times 10^{-3}\ \mathrm{cm} = 9.568\ \mu\mathrm{m}$$

is required (and 19.136 μm for an average stress of −1 GPa).

The predictions of the present calculation can be compared with the experimental results obtained for 20 μm thick layers grown homoepitaxially on HPHT- or thick quasi-substrates synthesized by heteroepitaxy.[29] In these experiments, the value of n_{dis} varied over 3–4 orders between the different samples. Growth was performed at high gas pressure and rather low substrate temperature in order to induce high compressive stress (850 °C, ≈200 mbar, 8% CH_4/H_2). The sample with $n_{\mathrm{dis}} = 1.8 \times 10^8\ \mathrm{cm}^{-2}$ showed a stress value of −1.2 GPa in reasonable accordance with

the present estimation. The film grown under identical conditions on a dislocation-rich quasi-substrate (6×10^9 cm^{-2}) reached −5.1 GPa at a thickness of only 6 μm.[29]

For the synthesis of thick diamond crystals, this extraordinarily high sensitivity of dislocation-rich crystals to the generation of growth stress demands conditions close to the zero-stress temperature equivalent to $|f| \ll 1$.

Due to the interaction of dislocations, resulting in annihilation or merging, the dislocation density is not a constant value but decreases monotonically with film thickness. Thus, built up of strain should vary in a proportional way. Based on the typical evolution of the dislocation density of a heteroepitaxial diamond film grown on Ir/YSZ/Si(001), roughly given by $n_{\mathrm{dis}}(d) \propto \frac{1}{d}$ with d being the film thickness,[31] $|\varepsilon_{xx}|$ will not increase $\propto z$ but sub-linearly. The experimentally found correlation $n_{\mathrm{dis}}(z)$ was fitted by the relationship,

$$n_{\mathrm{dis}}(z) = \frac{D_0}{z} = \frac{5 \times 10^6\ \mathrm{cm}^{-1}}{z}. \tag{19}$$

This yields a modified increase in the surface area A (number of lattice cells),

$$\frac{dA}{dz} = f\frac{1}{2}A_0 n_{\mathrm{dis}} a_0 = \frac{1}{2} f A_0 \frac{D_0}{z} a_0. \tag{20}$$

After integration, we obtain

$$A(z) = C_0 + \frac{1}{2} f A_0 D_0 a_0 \ln(z). \tag{21}$$

In order to avoid the singularity, the validity of this relationship is limited to the range $\{1\ \mu\mathrm{m}, \infty\}$. A film of thickness d starts at 1 μm and the position of the growth surface is at $d + 1\ \mu$m.

With $A(1\ \mu\mathrm{m}) = A_0$ and the selection $f = 0.1$, the value C_0 can be determined,

$$C_0 = A_0\left(1 - \frac{1}{2} f A_0 D_0 a_0 \ln(z)\right),$$

$$C_0 = A_0(1 + 0.0821 - 8.92 \times 10^{-3} \ln(\mathrm{cm})),$$

$$A(z) = A_0\left(1 + 0.0821 + 8.92 \times 10^{-3} \ln\left(\frac{z}{\mathrm{cm}}\right)\right).$$

Thus, for z = {1 μm, 501 μm}, we obtain

$$\varepsilon_{xx}(z) = -\frac{1}{2}\frac{\Delta A}{A_0} = -0.04105 - 4.46 \times 10^{-3} \ln\left(\frac{z}{\mathrm{cm}}\right)$$
$$= -4.46 \times 10^{-3} \ln\left(\frac{z}{\mu\mathrm{m}}\right). \tag{22}$$

This strain profile for inhibited deflection is calculated under the assumption that stress built up does not counteract dislocation bending. For a 500 μm thick layer, the stress at the surface (z = 501 μm) amounts to

$$\sigma_{xx} = \frac{1}{(s_{11} + s_{12})}\varepsilon_{xx} = E'\varepsilon_{xx}(501\ \mu\mathrm{m})$$
$$= -1172\ \mathrm{GPa} \times 4.46 \times 10^{-3} \times 6.217$$
$$= -32.49\ \mathrm{GPa},$$

with E' being the biaxial modulus for symmetric biaxial stress in the (001) plane.

Inhibited deflection and expansion is experimentally unrealistic, but it is rather helpful to find a solution for the radius and strain/stress profile that result in the other extreme case of free deflection and expansion. This adds a deformation $\varepsilon_{\mathrm{bend}}$ with

$$\varepsilon_{xx}^{\mathrm{bend}}(z) = \varepsilon_0 + C_{\mathrm{bend}} z. \tag{23}$$

Thus, the deformation profile changes to

$$\varepsilon_{xx}^{\mathrm{freedefl}}(z) = \varepsilon_{xx}(z) + \varepsilon_{xx}^{\mathrm{bend}}(z)$$
$$= -4.46 \times 10^{-3} \ln\left(\frac{z}{\mu\mathrm{m}}\right) + \varepsilon_0 + C_{\mathrm{bend}} z. \tag{24}$$

The values of the unknown constants ε_0 and C_{bend} can be found by applying the two boundary conditions of force F and momentum M balance.[32,33] Due to the absence of external forces, this means

$$F = \int_{1\mu\mathrm{m}}^{d+1\mu\mathrm{m}} \sigma(z)dz = 0 \text{ and } M = \int_{-d/2}^{+d/2} z_n \sigma(z_n) dz_n = 0. \tag{25}$$

z_n is the shifted z-axis with $z_n = 0$ at the position of the neutral plane. For a homogenous material, the neutral axis is in the center at $z = \frac{d}{2} + 1\ \mu\mathrm{m} = 251\ \mu\mathrm{m}$. Using the relationship $z_n = z - 251\ \mu$m, $dz = dz_n$ and $\sigma_{xx} = E'\varepsilon_{xx}$, we obtain the two equations:

$$0 = E'\int_{1\mu\mathrm{m}}^{d+1\mu\mathrm{m}} \varepsilon_{xx}^{\mathrm{freedefl}}(z)dz$$
$$= E'\int_{1\mu\mathrm{m}}^{d+1\mu\mathrm{m}} -4.46 \times 10^{-3} \ln\left(\frac{z}{\mu\mathrm{m}}\right) + \varepsilon_0 + C_{\mathrm{bend}} z dz \tag{26}$$

and

$$0 = \int_{1\mu\mathrm{m}}^{d+1\mu\mathrm{m}} \varepsilon_{xx}^{\mathrm{freedefl}}(z) \times (z - 251\ \mu\mathrm{m}) + \varepsilon_0(z - 251\ \mu\mathrm{m})$$
$$+ C_{\mathrm{bend}} z(z - 251\ \mu\mathrm{m})dz. \tag{27}$$

Calculation of the two definite integrals yields the conditional equations:

$$0 = -11.66 + 500\varepsilon_0 + 1.255 \times 10^5\ \mu\mathrm{m}\, C_{\mathrm{bend}}$$

and

$$0 = -272.94 - 0.5\,\varepsilon_0 + 1.0353625 \times 10^7\ \mu\text{m}\ C_{\text{bend}}.$$

Solving the system of equations yields

$$\varepsilon_0 = 0.01670 \text{ and } C_{\text{bend}} = 2.63626 \times 10^{-5}\,\frac{1}{\mu\text{m}} = 26.36\,\frac{1}{\text{m}}.$$

The different strain profiles according to (22)–(24) are summarized in Fig. 4.

The profile $\varepsilon_{xx}(z)$ for inhibited deflection and expansion is completely in the negative range equivalent to compressive stress. The curvature $C_{\text{bend}} = 26.36\,\frac{1}{\text{m}}$ yields a radius R of only 3.8 cm. Free deflection reduces strain and stress significantly. Inside the crystal (between z = 61 and 364 μm), it is still compressive with a stress maximum of −2.0 GPa at z = 170 μm. In contrast, at the bottom and upper surface, free bending results in tensile stress of nearly +20 (z = 1 μm) and +2.55 GPa (z = 501 μm). Thus, at two z-positions inside the crystal the stress changes its sign.

The following conclusions can be drawn:

(a) The fact that the strain profile changes its sign twice inside the crystal as shown in Fig. 4 is a direct consequence of the continuous structural improvement given by $n_{\text{dis}}(z) \propto \frac{1}{z}$.

(b) The authors of Ref. 10 have recently performed high precision lattice constant measurements by in-plane x-ray diffraction on both surfaces of heteroepitaxial diamond samples after release from the Ir/MgO or Ir/sapphire growth substrate, respectively. They always obtained tensile strain at both surfaces equivalent to tensile stress of several tenths of a gigapascal. The observation of stress with identical sign on both surfaces is in clear accordance with the present calculations.

(c) Early experiments on the multilayer system diamond/Ir/YSZ/Si in the authors lab at 850 °C and 200 mbar had often resulted in internal cracks of the diamond layers with a thickness in the range of 100 μm. These cracks running along (111) cleavage planes with a tilt angle of 54° started at the substrate surface and ended inside the film, while the growth surface of the diamond was completely intact.[34] The tensile stress that caused these cracks can now be understood on the base of the profiles shown in Fig. 4.

(d) The stress amplitudes found in the calculations for $f = 0.1$ would certainly not facilitate growth of intact layers with thicknesses in the mm-range. Thus, the experimental conditions are usually much closer to the zero-stress temperature. The full theory including f and d as variable parameters is described in Appendix A.

(e) In Appendix B, the bending radius and the stress profile of a freestanding 125 μm thick heteroepitaxial diamond film have been analyzed by μ-Raman spectroscopy in order to compare the results with the predictions of the present theory. The fits yield low f values of 8.5×10^{-4} and 4.6×10^{-4}, respectively.

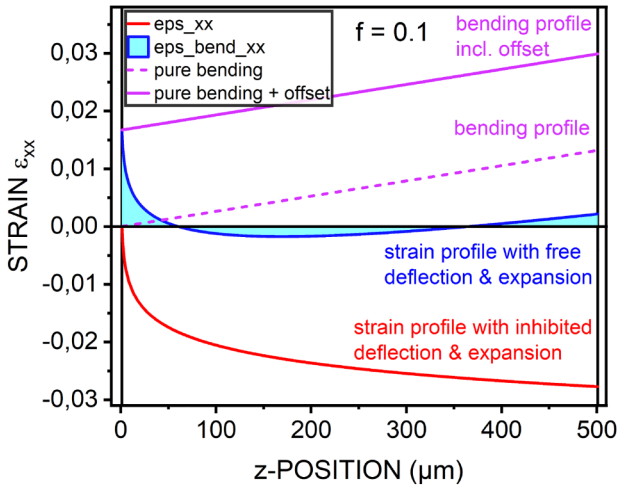

FIG. 4. Calculated strain profiles $\varepsilon_{xx}(z)$ for inhibited deflection and expansion, $\varepsilon_{xx}^{\text{bend}}(z)$ for the pure bending and $\varepsilon_{xx}^{\text{freedefl}}(z)$, the resulting curve for free deflection and expansion. The calculation is based on a dislocation profile $n_{\text{dis}}(z) = 5 \times 10^6\ \text{cm}^{-1}\,\frac{1}{z}$ starting at 1 μm, a value $f = 0.1$ and a film thickness of 500 μm.

IV. THE ROLE OF PLASTICITY

So far, all the considerations were limited to the elastic deformation of the substrate. Even the continuous crystal lattice deformation of the growing diamond due to stress formation by the effective climb of dislocations does not involve any real dislocation movement: according to the present understanding of the responsible mechanisms, it is exclusively controlled by the kinetics of atomistic growth processes at the diamond surface. Below the surface, dislocations are considered immobile during growth.

However, various experimental findings point to a crucial role of plastic processes. For instance, a series of 13 crystals formerly grown in the authors' lab on Ir/YSZ/Si(001) substrates up to final thicknesses of 1.1–1.2 mm showed radii scattering between 1.2 and 4.9 m. The average value was 2.8 ± 1.37 m. Two crystals had even a combination of convex and concave bending in the two perpendicular directions, respectively. The process conditions for the growth of the crystals were virtually identical. As a consequence, differences in crystal growth could not provide a convincing explanation for this large scatter. In addition, the 3 mm thick silicon substrates were usually heavily deformed plastically after the process.

In the recent *in situ* study by Sawabe's group,[8] the curvature of the freestanding diamond grown on MgO was nearly eight times higher than the initial curvature of the Ir/MgO substrate measured *in situ* at the beginning of the diamond deposition process (i.e., 8.5 vs 1.1 1/m, respectively). This provides compelling evidence that during long-term CVD growth, additional processes take place in the diamond film and the substrate, which can change the final shape of thick freestanding diamond discs, fundamentally.

The considered oxides as well as diamond and silicon are classified as brittle at room temperature (RT). They show a linear stress–strain curve with negligible plastic deformation before fracture. At common diamond growth conditions, the situation is different. Silicon has crossed its brittle–ductile transition at ≈550 °C,

which means that the fracture mode has changed.[35] Instead of cracking, the material starts irreversible plastic deformations. In single crystals, this is intimately connected with dislocation movement. The critical stress values define the yield strength, a quantity that shows a complex dependency on various parameters such as temperature, crystal anisotropy, loading axis, strain rate, and the presence of dislocations. A compilation of strength and plasticity data for the relevant materials is given in Table II.

The onset of plastic deformation in diamond in the temperature range between 900 and 1100 °C required pressures between 6 and 1 GPa, respectively.[36]

As a supplement to Table II, the results from four-point flexure strength measurements on sapphire bars at 1000 °C are mentioned, which yielded values between 169 and 782 MPa for different orientations. The lowest value is for samples with the *c*-axis under tension.[41]

According to this survey of mechanical data, Si and MgO are ductile at 1000 °C with a yield strength comparable to single crystals of pure soft metals like copper[42] or aluminum[43] at room temperature, i.e., up to several 10 MPa, only. In contrast, diamond and sapphire are still brittle and their tensile strength at deposition temperature is 1–2 orders of magnitude higher.

This results in the following basic scenarios for the growth of thick diamond layers ($\gg 100\,\mu$m) on one of the considered substrates:

(1) During the first microns of growth on Ir/Al_2O_3, the diamond follows the external shape of the substrate surface, which means that it adopts a radius of 0.6 m under an assumed heat flux density of 10^6 W/cm^2. For lower heat load, the radius will be accordingly higher and the curvature lower. In case the growth conditions are tuned to minimize the formation of growth stress (see Sec. III), stable growth up to thicknesses in the millimeter range should be possible. After cooldown, diamond radii close to the values of the pure substrate at the beginning of the growth process are expected. This is apparently the case for the values of ≈1 m reported in Refs. 7 and 9. In the case of less appropriate growth conditions, huge stress (in the GPa range) is built up and strong bending in the diamond and cracking of film and/or substrate is often the result.

(2) Diamond growth at ≈1000 °C on Ir/MgO or silicon-based substrates is much more delicate. Only when the soft spot of zero stress is hit rather precisely, the diamond can grow virtually stress-free and it will adopt the curvature of the substrate, which is ten times higher for MgO than for Si (see Sec. II).

(3) Minor growth stress in the diamond deposited on Ir/MgO or Ir/YSZ/Si will immediately start to exert forces on the soft substrates trying to change their bending state. In contrast to the bending induced by the temperature gradient, this bending is accompanied by stress built-up in the substrates. Since their yield strength at 1000 °C is about 2 orders of magnitude lower than that of diamond, even for diamond layers significantly thinner than the substrate, plastic flow will start first inside the substrates. In addition, this deformation releases the stress inside the diamond layer before it can reach the threshold for yielding. The process parameter dependent bending of the dislocations (effective climb of dislocations) will continue, unhinderedly resulting in the final bending and internal strain distribution as calculated in Sec. III for the case of free deflection. This is apparently the situation described in Ref. 8 where the curvature of the diamond layer was eight times higher than the initial surface curvature of the substrate. In the authors group, unfavorable crystals with high curvatures had radii of 0.5–1 m^{-1}, which is again nearly an order of magnitude higher than the value expected from the heat flow induced curvature of the silicon substrate.

(4) Under growth conditions for compressive stress formation performed on a soft substrate like silicon, the high tensile stress in the diamond close to the interface as shown in Fig. 4 can even cause brittle fracture inside the diamond.

TABLE II. Brittle–ductile transition temperatures T_c and yield stress values for silicon, Al_2O_3, MgO, and diamond.

Material	Brittle–ductile transition temperature T_c (°C)	Yield stress (1000 °C) (MPa)
Si	545[a]	4–18[b]
Al_2O_3	1034–1150[c]	See the text
MgO	350[d]	28[e]
Diamond	≈900–1100[f]	≈3000[f]

[a]Ref. 35.
[b]Ref. 37.
[c]T_c values of Al_2O_3 data are for an A-oriented specimen and strain rates of 4.2×10^{-7} and 4.2×10^{-6}, respectively.[38]
[d]T_c for MgO with ⟨111⟩ loading axis and the activation of the {100}⟨110⟩ slip system.[39]
[e]Yield stress for MgO with loading in the ⟨100⟩ direction with 0.14 MPa/s.[40]
[f]Ref. 36.

V. DEFORMATION DURING COOLDOWN

During cooldown, the difference in CTEs will create a new source of stress. The magnitude of this extrinsic stress increases continuously with decreasing temperature $\propto(T_{\text{depositon}} - T)$. However, at the same time, the yield stress increases for the substrate as well as for the diamond coating. Diamond's yield stress will always surpass that of the substrate. It is, therefore, rather implausible to expect any further plastic deformation of the diamond during this final step. The high strain rate (due to fast cooldown) further supports this interpretation.

VI. POTENTIAL SOLUTIONS FOR THE CURVATURE PROBLEM

Lowering the gas pressure to decrease the heat flow is an obvious but impracticable strategy to reduce the initial bending of the substrate. Lower pressure reduces the growth rate drastically so that this approach seems economically not feasible.

To obtain diamond growth in a high-power plasma on a flat substrate, the wafer should be pre-shaped with a curvature in the opposite direction, i.e., concave at the deposition surface. The vertical temperature gradient established by the heat flow can then create a flat substrate. For this pre-shaping, two different

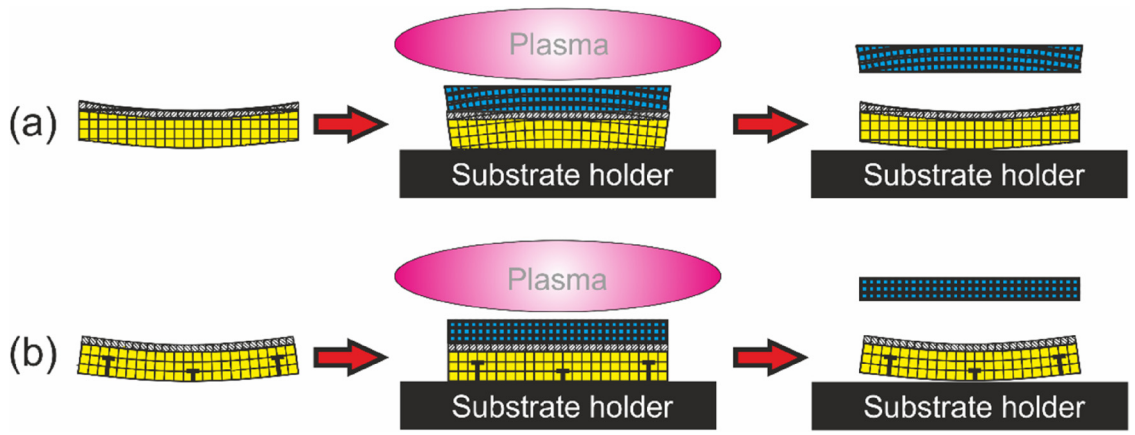

FIG. 5. Pre-shaping of substrates as a strategy for the synthesis of flat diamond wafers. (a) A substrate wafer with a concave surface (and the corresponding convex backside) with an epitaxial Ir layer grown on top. It turns flat in the plasma and facilitates the growth of an externally flat diamond crystal. (b) A plastically deformed base substrate (see dislocations due to plastic deformation) can produce an externally and crystallographically flat diamond wafer. For details, see text.

approaches can be distinguished. As shown in Fig. 5(a), a flat single crystal can obtain a spherical shape by grinding and polishing. Then, Ir is deposited epitaxially on the concave surface. Under the influence of the plasma, the wafer becomes flat. In this case, the final diamond will have an externally flat surface. However, the crystal lattice will still be bent as before: the direction of the reciprocal lattice vector of the crystallographic surface plane continuously varies across the diameter of the wafer. Figure 5(b) describes a plastically deformed single crystal for which the crystallographic plane at the local surface is everywhere identical over the whole spherical substrate surface. For silicon, the feasibility of such a structure with an extremely small radius of only 10 cm has been demonstrated.[44]

Due to their high symmetry, the procedure works best for cubic crystals. For trigonal crystals like Al_2O_3, the concept should be feasible for *c*-axis orientation. For other orientations, a non-spherical shape with two bending radii in two orthogonal directions is required.

VII. SUMMARY AND CONCLUSIONS

Fabrication of diamond electronic devices using established methods in the semiconductor industry demands plane-parallel wafers. In this work, wafer bow has been analyzed for the synthesis by heteroepitaxy on various base substrates. The calculations reveal that the strong curvature 1/R of the substrates already occurs before diamond growth starts. Its scaling $\frac{1}{R} = \frac{\alpha}{\lambda} J$ shows that the extraordinarily high heat flow through the substrate in high-temperature plasma discharges is responsible for this specific problem in diamond synthesis. Decreasing the plasma temperature by lowering the pressure does not provide a viable solution due to the involved drastic drop in the growth rate.

A figure of merit for substrate materials facilitating minimum wafer bow is given by λ/α. In this aspect, for deposition at 1000 °C, silicon outperforms $Al_2O_3(0001)$ and MgO by factors of 8.6 and 10.7, respectively. These numbers highlight the superiority of Si based multilayer substrates.

The heat flow induced bow can be compensated for by pre-shaping the substrates so that they turn flat when exposed to the plasma. An external pre-shaping of the single crystal substrate can result in an externally flat diamond wafer. However, the crystal lattice still changes its orientation continuously along the wafer diameter as before. The second approach of plastic deformation has the potential to generate externally and internally flat single crystal diamond wafers.

In both cases, the compensation can only work when diamond growth is performed in a way that virtually no internal stress is formed. Via the process of effective climb of dislocations, huge values of compressive or tensile stress can be generated by growth at accordingly low or high temperatures, respectively. The higher the dislocation density the more sensitive is the growing film to the formation of intrinsic stress. Minimization is possible for highly symmetric growth surfaces by the choice of the correct temperature. In contrast, stress tensor analysis for (111) off-axis grown diamond has previously shown that in-plane tensile and compressive components can coexist, which seems to exclude the existence of a zero-stress temperature.

Strain and bending as a consequence of compressive growth stress formation have been calculated within a simple model, which assumes that strain increase with thickness is proportional to the dislocation density $n_{dis}(z)$. The proportionality factor f is a function of growth temperature. The calculations performed for $n_{dis} \propto \frac{1}{d}$ under the condition of free deflection and for compressive stress formation predict a compressive region inside the crystal and tensile stress at both surfaces. Even for strongly bent bulk crystals synthesized under constant conditions, the absolute value of residual stress inside the crystals is very low. It would ultimately disappear in the case of a constant dislocation density. Comparison with the literature and own measurements confirm all these trends. Factor f is on the order of one at low temperature where maximum stress of several GPa

compressive stress is measured after several micron growth. For the realization of flat bulk crystals, f should be in the 10^{-5} range.

Finally, the role of plastic deformation processes was considered. The brittle/ductile transition and the yield stress at deposition temperature are the relevant parameters. Diamond and Al_2O_3 are still rather hard sustaining stress in the GPa range even at 1000 °C. In contrast, silicon and MgO are very soft at this temperature, which means that they can easily be deformed by the diamond growing on top. Diamond grows on these substrates approximately under free-deflection conditions. There are indications that even diamond can deform plastically under extreme growth conditions. Significant contributions from stress induced plastic deformation during cooldown due to differences in CTEs are largely ruled out.

ACKNOWLEDGMENTS

We acknowledge the financial support by the German Research Foundation DFG (No. 453637298) and colleagues from Augsburg Diamond Technology GmbH for the provision of diamond samples and curvature data.

AUTHOR DECLARATIONS

Conflict of Interest

Theodor Peter has no conflict of interest. Matthias Schreck has German patent pending (10 2022 205 081.9, filed 20.05.2022).

Author Contributions

Matthias Schreck: Conceptualization (lead); Data curation (equal); Formal analysis (equal); Funding acquisition (lead); Investigation (equal); Methodology (lead); Project administration (lead); Writing – original draft (lead); Writing – review & editing (equal). **Theodor Peter:** Data curation (equal); Formal analysis (equal); Investigation (equal); Writing – review & editing (equal).

DATA AVAILABILITY

The data that support the findings of this study are available from the corresponding author on request.

APPENDIX A: CALCULATION OF BENDING AND STRAIN WITH VARIABLES f AND d

In Sec. III, estimations on the maximum amplitude of growth stress induced by the effective climb of dislocations mechanism were done for $f = 1$. The subsequent calculation of bending and strain profile for a diamond layer with $d = 500\,\mu$m was performed for $n_{\mathrm{dis}}(z) = \frac{5\times10^6\ \mathrm{cm}^{-1}}{z}$ and $f = 0.1$. In this appendix, we present the general solution for the two constants ε_0 and C_{bend} in Eq. (24) by performing the calculation with f and d as free parameters:

$$\varepsilon_0 = \frac{fD_0a_0}{2d^3}\left(\frac{1}{2}d^3\ln(d+1) - \frac{5}{4}d^3 + 2d^2\ln(d+1) - 3d^2 + \frac{9}{2}d\ln(d+1) + 3\ln(d+1) - 3d\right) \quad \text{(A1)}$$

and

$$C_{\mathrm{bend}} = \frac{fD_0a_0}{d^3}\left(\frac{3}{4}d^2 - \frac{3}{2}d\,\ln(d+1) - \frac{3}{2}\ln(d+1) + \frac{3}{2}d\right). \quad \text{(A2)}$$

The result was obtained with a Casio fx-CP400 and was verified for the special case of d = 500 μm and $f = 0.1$.

APPENDIX B: ANALYSIS OF THE BENDING RADIUS AND STRESS PROFILE FOR A 125 μM THICK HETEROEPITAXIAL DIAMOND SAMPLE

To check the theoretical considerations, a freestanding strongly bent heteroepitaxial diamond sample with a thickness of $125 \pm 0.6\,\mu$m as deduced from white light interference measurements was investigated. Its bending radius was measured by laser microscopy. Values of $R_{\mathrm{exp}} = 163 \pm 9$ mm on the nucleation side and 156 ± 6 mm on the growth side with an average of 160 mm were obtained.

μ-Raman spectroscopy with high spectral resolution (0.4 cm^{-1}) and confocal optics was performed with a T64000 triple spectrometer. To calibrate the spectral position, the extremely narrow and accurate plasma lines of a spectral lamp were fed during every measurement together with the Raman light into the entrance slit of the spectrometer. Maps of $6 \times 6 = 36$ spots with a 10 μm-spacing were measured in different depths. Every spectrum was first corrected using the position of the nearest plasma line. Then, all the spectra of a map were summed up. Peak position and width of the sum profile were then derived by peak fitting. Finally, the stress for a given depth was calculated assuming a plane biaxial stress state with a factor of −0.61 GPa/cm^{-1} for the conversion between the Raman line shift and stress value.[45]

The blue data points in Fig. 6 represent the stress values $\sigma_{xx}(z)$ as derived from the Raman shifts. They vary roughly between 0.1 and 0.2 GPa, which means that the whole crystal is under tension. Basically, impurities and defects widening the crystal lattice could generate such an effect. The same applies to minor systematic errors in the determination of the Raman peak position. A shift by −0.0976 GPa (equivalent to a Raman peak shift by 0.160 cm^{-1}) yields a depth distribution of the stress values in which tensile regions are exactly balanced by volumes under compression, thus guaranteeing a force equilibrium $\sum_i \sigma_{xx}(z_i) = 0$ inside the whole crystal.

Comparison of the measured data with theoretical predictions is possible in two different ways: using Eq. (A2), f can directly be calculated from the experimentally determined curvature $C_{\mathrm{bend}} = \frac{1}{R_{\mathrm{exp}}} = 6.25\ \mathrm{m}^{-1}$, yielding $f = 6.0 \times 10^{-3}$. Then, ε_0 is calculated via Eq. (A1) from f. Insertion of C_{bend} and ε_0 in Eq. (23) yields the theoretical curve $\sigma_{xx}(z) = E'\varepsilon_{xx}^{\mathrm{freedefl}}(z)$ without any free fit parameters [see Fig. 6(a)]. In the second approach, f is a free fit parameter to get the best approximation to the shifted experimental data. Values of $C_{\mathrm{bend}} = 0.886\ \mathrm{m}^{-1}$ equivalent to $R = 1.13$ m and $f = 8.5 \times 10^{-4}$ are obtained for $n_{\mathrm{dis}}(z) \propto \frac{1}{z}$ [see Fig. 6(b)].

The two results differ by a factor of ≈7. In addition to the $\propto z^{-1}$ behavior reported for n_{dis} in Ref. 31, a slower decrease $\propto z^{-0.82}$ and $\propto z^{-0.94}$ has been observed in other investigations.[46] Therefore, we performed the theoretical calculations also for $z^{-0.5}$. The result

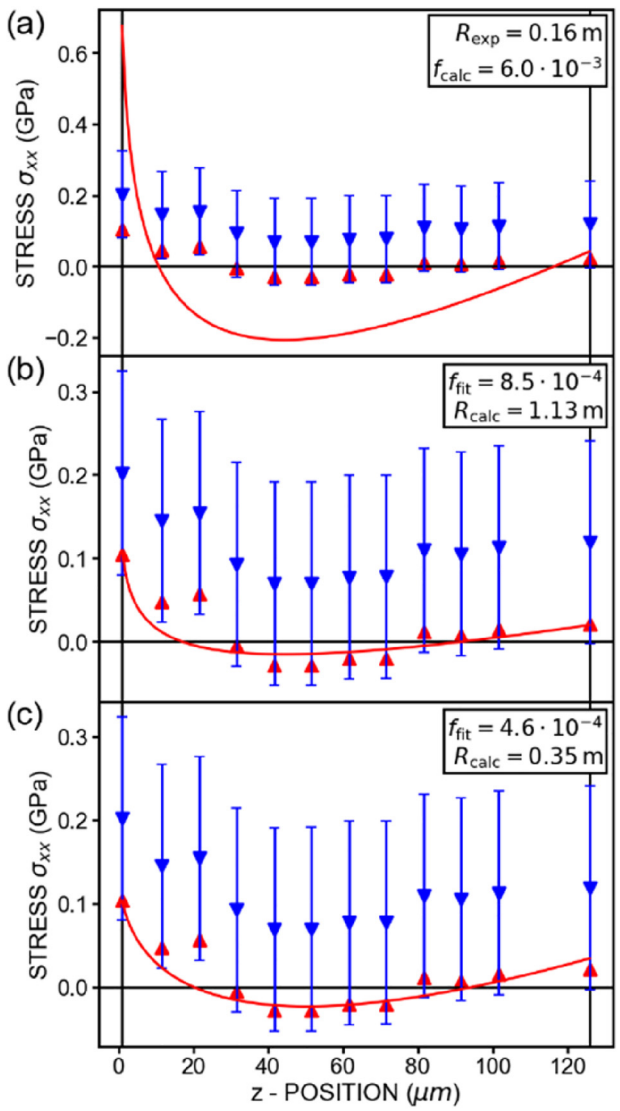

FIG. 6. Stress profile inside a 125 μm thick heteroepitaxial diamond layer after the removal of the Ir/YSZ/Si substrate. Blue data points stem directly from μ-Raman spectra. Red data points are shifted by −0.0976 GPa. (a) Stress curve $\sigma_{xx}(z)$ calculated from R_{exp}. (b) Fit of $\sigma_{xx}(z)$ by variation in f (for $n_{dis}(z) = \frac{5\times10^{6}\ \mathrm{cm}^{-1}}{z}$). (c) Fit of $\sigma_{xx}(z)$ by the variation in f (for $n_{dis}(z) = \frac{5\times10^{8}\ \mathrm{cm}^{-3/2}}{\sqrt{z}}$).

shown in Fig. 6(c) yields $R = 0.35$ m and $f = 4.6 \times 10^{-4}$. The difference between R_{exp} and the R value deduced from the calculation has now reduced to a factor ≈2, indicating that the drop in dislocation density may actually be slower.

For a final assessment of the result, one has to mention that the initial bending of the substrate caused by the heat load of the plasma (see Sec. II) is not considered in our calculations.

Summarizing these results, we conclude that our considerations facilitate the derivation of a rough number for the f-value.

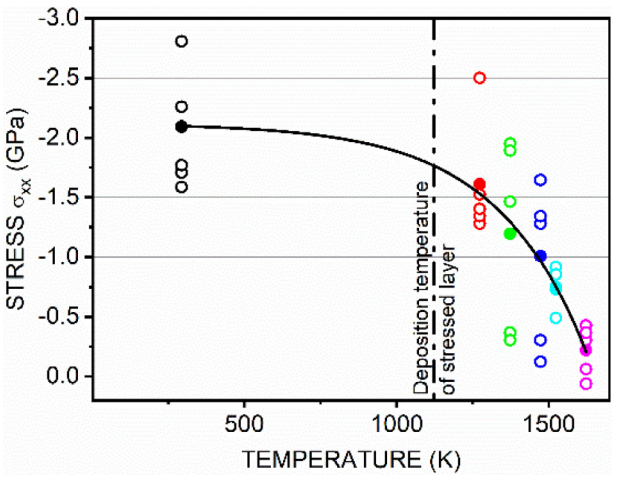

FIG. 7. Change in biaxial stress for a 20 μm thick layer on a Ib substrate induced by stepwise annealing for always 5 h at different temperatures. Open and full symbols indicate the single measurements and the average value, respectively.

Even for a heavily bent crystal with a radius well below 1 m, this f is more than 2–3 orders of magnitude lower than the f-value required to explain the stress formation of several GPa in 20 μm thick homoepitaxial layers (see discussion in Sec. III). The envisaged synthesis of extremely flat crystals will require f values in the 10^{-5} range. Our analysis can conclusively explain the identical sign of the stress on both faces of bent crystals. Finally, it makes understandable the low residual stress values consistently found by Raman and HRXRD measurements in heavily bent crystals. This fact also explains the difficulty to correlate experimental and simulated stress values with decent accuracy.

APPENDIX C: RELAXATION OF COMPRESSIVE STRESS IN THIN HOMOEPITAXIAL DIAMOND LAYERS BY HIGH-TEMPERATURE ANNEALING

In a former PhD thesis,[47] a 20 μm thick compressively stressed diamond layer was grown homoepitaxially on an I HPHT crystal at 850 °C, 200 mbar, and 8% CH_4/H_2. In order to facilitate stress built-up, the growth surface was pretreated by a short bias enhanced growth step, which caused the nucleation of dislocations with $n_{dis} > 10^8$ cm^{-2}. Figure 7 shows the change in stress induced by subsequent high-temperature annealing steps. The measurements were done by μ-Raman spectroscopy. To derive the residual stress from the measured diamond Raman peak shift, a symmetric in-plane biaxial stress state was assumed.

The derived residual stress remaining after treatment at different temperatures is conform with the onset of plastic deformation reported in Ref. 36.

REFERENCES

[1] *Power Electronics Device Application of Diamond Semiconductors*, edited by S. Koizumi, H. Umezawa, J. Pernot, and M. Suzuki (Elsevier Ltd., 2018).

[2]M. Schreck, "Growth of single crystal diamond wafers for future device applications," in *Wide Bandgap Semiconductors for Power Electronics*, edited by P. Wellmann, N. Ohtani, and R. Rupp (Wiley-VCH, Weinheim, 2022), pp. 585–631.
[3]M. Schreck, S. Gsell, R. Brescia, and M. Fischer, "Ion bombardment induced buried lateral growth: The key mechanism for the synthesis of single crystal diamond wafers," Sci. Rep. **7**, 44462 (2017).
[4]A. K. Freund, S. Gsell, M. Fischer, M. Schreck, K. H. Andersen, P. Courtois, G. Borchert, and M. Skoulatos, "Diamond mosaic crystals for neutron instrumentation: First experimental results," Nucl. Instrum. Methods Phys. Res., B **634**, S28–S36 (2011).
[5]M. Fischer, A. K. Freund, S. Gsell, M. Schreck, P. Courtois, C. Stehl, G. Borchert, A. Ofner, M. Skoulatos, and K. H. Andersen, "Structural analysis of diamond mosaic crystals for neutron monochromators using synchrotron radiation," Diamond Relat. Mater. **37**, 41 (2013).
[6]P. Courtois, M. T. Fernandez-Diaz, G. Nenert, K. H. Andersen, A. K. Freund, S. Gsell, M. Fischer, M. Schreck, P. Link, and M. Meven, "The first prototype diamond monochromator at the Institut Laue-Langevin," J. Phys.: Conf. Ser. **528**, 012001 (2014).
[7]S.-W. Kim, Y. Kawamata, R. Takaya, K. Koyama, and M. Kasu, "Growth of high-quality one-inch free-standing heteroepitaxial (001) diamond on (11–20) sapphire substrate," Appl. Phys. Lett. **117**, 202102 (2020).
[8]H. Aida, T. Ihara, R. Oshima, Y. Kimura, and A. Sawabe, "Analysis of external surface and internal lattice curvatures of freestanding heteroepitaxial diamond grown on an Ir (001)/MgO (001) substrate," Diamond Relat. Mater. **136**, 110026 (2023).
[9]S.-W. Kim, R. Takaya, S. Hirano, and M. Kasu, "Two-inch high-quality (001) diamond heteroepitaxial growth on sapphire (11$\bar{2}$0) misoriented substrate by step-flow mode," Appl. Phys. Express **14**, 115501 (2021).
[10]M. Kasu, R. Takaya, and S.-W. Kim, "Growth of high-quality inch-diameter heteroepitaxial diamond layers on sapphire substrates in comparison to MgO substrates," Diamond Relat. Mater. **126**, 109086 (2022).
[11]M. K. Kelly, R. P. Vaudo, V. M. Phanse, L. Görgens, O. Ambacher, and M. Stutzmann, "Large free-standing GaN substrates by hydride vapor phase epitaxy and laser-induced liftoff," Jpn. J. Appl. Phys. **38**, L217 (1999).
[12]B. Monemar, H. Larsson, C. Hemmingsson, I. G. Ivanov, and D. Gogova, "Growth of thick GaN layers with hydride vapour phase epitaxy," J. Cryst. Growth **281**, 17 (2005).
[13]K. Yamane, M. Ueno, H. Furuya, N. Okada, and K. Tadatomo, "Successful natural stress-induced separation of hydride vapor phase epitaxy-grown GaN layers on sapphire substrates," J. Cryst. Growth **358**, 1 (2012).
[14]F. Brunner, A. Knauer, T. Schenk, M. Weyers, and J.-T. Zettler, "Quantitative analysis of *in situ* wafer bowing measurements for III-nitride growth on sapphire," J. Cryst. Growth **310**, 2432 (2008).
[15]F. Silva, K. Hassouni, X. Bonnin, and A. Gicquel, "Microwave engineering of plasma-assisted CVD reactors for diamond deposition," J. Phys.: Condens. Matter **21**, 364202 (2009).
[16]C. Y. Ho, R. W. Powell, and P. E. Liley, "Thermal conductivity of the elements," J. Phys. Chem. Ref. Data **1**, 279 (1972).
[17]G. K. White and M. L. Minges, "Thermophysical properties of some key solids: An update," Int. J. Thermophys. **18**, 1269 (1997).
[18]D. G. Cahill, S.-M. Lee, and T. I. Selinder, "Thermal conductivity of κ-Al_2O_3 and α-Al_2O_3 wear-resistant coatings," J. Appl. Phys. **83**, 5783 (1998).
[19]D. C. Harris *et al.*, "Properties of an infrared-transparent MgO:Y_2O_3 nanocomposite," J. Am. Ceram. Soc. **96**, 3828 (2013).
[20]Y. S. Touloukian, R. K. Kirby, R. E. Taylor, and T. Y. R. Lee, "Thermal expansion nonmetallic solids," in *Thermophysical Properties of Matter* (Purdue Research Foundation, 1977), Vol. 13.
[21]J. W. Vandersande, "Thermal conductivity of natural-isotope diamond," in *Properties and Growth of Diamond*, edited by G. Davies (Inspec, London, 1994), p. 33.
[22]G. Abadias, E. Chason, J. Keckes, M. Sebastiani, G. B. Thompson, E. Barthel, G. L. Doll, C. E. Murray, C. H. Stoessel, and L. Martinu, "Review article: Stress in thins films and coatings: Current status, challenges and prospects," J. Vac. Sci. Technol. A **36**, 020801 (2018).
[23]H. Windischmann, "Intrinsic stress in sputter-deposited thin films," Crit. Rev. Solid State Mater. Sci. **17**, 547 (1992).
[24]C. A. Davis, "A simple model for the formation of compressive stress in thin films by ion bombardment," Thin Solid Films **226**, 30 (1993).
[25]H. Windischmann, G. F. Epps, Y. Cong, and R. W. Collins, "Intrinsic stress in diamond films prepared by microwave plasma CVD," J. Appl. Phys. **69**, 2231–2237 (1991).
[26]M. Mermoux, B. Marcus, A. Crisci, A. Tajani, E. Gheeraert, and E. Bustarret, "Micro-Raman scattering from undoped and phosphorous-doped (111) homoepitaxial diamond films: Stress imaging of cracks," J. Appl. Phys. **97**, 043530 (2005).
[27]M. Fischer, S. Gsell, M. Schreck, and A. Bergmaier, "Growth sector dependence and mechanism of stress formation in epitaxial diamond growth," Appl. Phys. Lett. **100**, 041906 (2012).
[28]B.-C. Gallheber, M. Fischer, O. Klein, and M. Schreck, "Formation of huge in-plane anisotropy of intrinsic stress by off-axis growth of diamond," Appl. Phys. Lett. **109**, 141907 (2016).
[29]M. Schreck, M. Mayr, O. Klein, M. Fischer, S. Gsell, A. F. Sartori, and B.-C. Gallheber, "Multiple role of dislocations in the heteroepitaxial growth of diamond: A brief review," Phys. Status Solidi A **213**, 2028–2035 (2016).
[30]B.-C. Gallheber, O. Klein, M. Fischer, and M. Schreck, "Propagation of threading dislocations in heteroepitaxial diamond films with (111) orientation and their role in the formation of intrinsic stress," J. Appl. Phys. **121**, 225301 (2017).
[31]C. Stehl, M. Fischer, S. Gsell, E. Berdermann, M. S. Rahman, M. Traeger, O. Klein, and M. Schreck, "Efficiency of dislocation density reduction during heteroepitaxial growth of diamond for detector applications," Appl. Phys. Lett. **103**, 151905 (2013).
[32]T. W. Clyne and S. C. Gill, "Residual stresses in thermal spray coatings and their effect on interfacial adhesion: A review of recent work," J. Therm. Spray Technol. **5**, 401 (1996).
[33]T. W. Clyne, "Residual stresses in coated and layered systems," in *Encyclopedia of Materials: Science and Technology*, edited by K. H. J. Buschow, R. W. Cahn, M. C. Flemings, B. Ilschner, E. J. Kramer, S. Mahana, and P. Veyssière (Elsevier, 2001), pp. 8126–8134.
[34]D. Reuber, "Ramanmessungen an heteroepitaktischen Diamantschichten," Bachelor thesis (University of Augsburg, 2008) (in German).
[35]P. B. Hirsch and S. G. Roberts, "The brittle-ductile transition in silicon," Philos. Mag. A **64**, 55 (1991).
[36]R. C. DeVries, "Plastic deformation and work hardening of diamond," Mater. Res. Bull. **10**, 1193 (1975).
[37]H. Siethoff, H.-G. Brion, and W. Schröter, "A regime of the yield point of silicon at high temperatures," Appl. Phys. Lett. **75**, 1234–1236 (1999).
[38]H. S. Kim and S. Roberts, "Brittle-ductile transition and dislocation mobility in sapphire," J. Am. Ceram. Soc. **77**, 3099 (1994).
[39]C. O. Hulse, S. M. Copley, and J. A. Pask, "Effect of crystal orientation on plastic deformation of magnesium oxide," J. Am. Ceram. Soc. **46**, 317 (1963).
[40]C. O. Hulse and J. A. Pask, "Mechanical properties of magnesia single crystals in compression," J. Am. Ceram. Soc. **43**, 373 (1960).
[41]F. Schmid and D. C. Harris, "Effects of crystal orientation and temperature on the strength of sapphire," J. Am. Ceram. Soc. **81**, 885 (1998).
[42]F. W. Young, Jr., "On the yield stress of copper crystals," J. Appl. Phys. **33**, 963 (1962).
[43]S. Groh, E. B. Marin, M. F. Horstemeyer, and H. M. Zbib, "Multiscale modeling of the plasticity in an aluminum single crystal," Int. J. Plasticity **25**, 1456 (2009).
[44]K. Nakajima, K. Fujiwara, W. Pan, and H. Okuda, "Shaped silicon crystal wafers obtained by plastic deformation and their application to silicon crystal lenses," Nat. Mater. **4**, 47 (2005).
[45]Y. von Kaenel, J. Stiegler, J. Michler, and E. Blank, "Stress distribution in heteroepitaxial chemical vapor deposited diamond films," J. Appl. Phys. **81**, 1726 (1997).
[46]M. Schreck, P. Ščajev, M. Träger, M. Mayr, T. Grünwald, M. Fischer, and S. Gsell, "Charge carrier trapping by dislocations in single crystal diamond," J. Appl. Phys. **127**, 125102 (2020).
[47]M. Fischer, "Heteroepitaxie von Diamant auf Iridium/YSZ/Silizium: Untersuchungen zu Keimbildung, Wachstum und Schichteigenschaften," PhD thesis (University of Augsburg, 2013) (in German).